01 Nov 2020

Calcium Sulfate-Containing Glass Polyalkenoate Cement for Revision Total Knee Arthroplasty Fixation

Leyla Hasandoost

Adel Alhalawani

Omar Rodriguez

Alireza Rahimnejad Yazdi

et. al. For a complete list of authors, see https://scholarsmine.mst.edu/che_bioeng_facwork/1074

Recommended Citation

L. Hasandoost et al., "Calcium Sulfate-Containing Glass Polyalkenoate Cement for Revision Total Knee Arthroplasty Fixation," *Journal of Biomedical Materials Research - Part B Applied Biomaterials*, vol. 108, no. 8, pp. 3356 - 3369, Wiley, Nov 2020.
The definitive version is available at https://doi.org/10.1002/jbm.b.34671

Received: 2 October 2019 | Revised: 18 April 2020 | Accepted: 3 June 2020

DOI: 10.1002/jbm.b.34671

ORIGINAL RESEARCH REPORT

Society For Biomaterials | WILEY

Calcium sulfate-containing glass polyalkenoate cement for revision total knee arthroplasty fixation

Leyla Hasandoost[1,2] | Adel Alhalawani[2,3] | Omar Rodriguez[2,3] | Alireza Rahimnejad Yazdi[2,3] | Paul Zalzal[4,5] | Emil H. Schemitsch[2,6] | Stephen D. Waldman[1,2,7] | Marcello Papini[1,3] | Mark R. Towler[1,2,3]

[1]Faculty of Engineering and Architectural Science, Biomedical Engineering Program, Ryerson University, Toronto, Ontario, Canada

[2]Li Ka Shing Knowledge Institute, St. Michael's Hospital, Toronto, Ontario, Canada

[3]Department of Mechanical & Industrial Engineering, Ryerson University, Toronto, Ontario, Canada

[4]Faculty of Health Sciences, Department of Surgery, McMaster University, Hamilton, Ontario, Canada

[5]Oakville Trafalgar Memorial Hospital, Oakville, Ontario, Canada

[6]Department of Surgery, University of Western Ontario, London, Ontario, Canada

[7]Department of Chemical Engineering, Ryerson University, Toronto, Ontario, Canada

Correspondence
Mark R. Towler, Department of Mechanical and Industrial Engineering, Faculty of Engineering and Architectural Science, 350 Victoria Street, Toronto, ON M5B 2K3, Canada.
Email: mtowler@ryerson.ca

Funding information
CIHR/NSERC-Collaborative Health Research Projects, Grant/Award Number: 356780-DAN

Abstract

Poly(methyl methacrylate) (PMMA) bone cement is used as a minor void filler in revision total knee arthroplasty (rTKA). The application of PMMA is indicated only for peripheral bone defects with less than 5 mm depth and that cover less than 50% of the bone surface. Treating bone defects with PMMA results in complications as a result of volumetric shrinkage, bone necrosis, and aseptic loosening. These concerns have driven the development of alternative bone cements. We report here on novel modified glass polyalkenoate cements (mGPCs) containing 1, 5 and 15 wt% calcium sulfate ($CaSO_4$) and how the modified cements' properties compare to those of PMMA used in rTKA. $CaSO_4$ is incorporated into the mGPC to improve both osteoconductivity and bioresorbability. The results confirm that the incorporation of $CaSO_4$ into mGPCs decreases the setting time and increases release of therapeutic ions such as Ca^{2+} and Zn^{2+} over 30 days of maturation in deionized (DI) water. Moreover, the compressive strength for 5 and 15 wt% $CaSO_4$ addition increased to over 30 MPa after 30 day maturation. Although the overall initial compressive strength of the mGPC (~ 30 MPa) is less than PMMA (~ 95 MPa), the compressive strength of mGPC is closer to that of cancellous bone (~ 1.2–7.8 MPa). $CaSO_4$ addition did not affect biaxial flexural strength. Fourier transform infrared analysis indicated no cross-linking between $CaSO_4$ and the GPC after 30 days. in vivo tests are required to determine the effects the modified GPCs as alternative on PMMA in rTKA.

KEYWORDS

bone cement, bone loss, calcium sulfate, glass polyalkenoate cement, PMMA, revision total knee arthroplasty

1 | INTRODUCTION

Failure of total knee arthroplasty (TKA) requires revision TKA (rTKA) to improve the function of the knee, reduce patient pain and manage both bone loss and infection (Fehring et al., 2008). According to the Canadian Institute for Health Information (CIHI), among 84,770 (35,945, excluding patella) rTKAs performed between 2012 and 2017, main reasons for revision were infection (38.4%), instability (22.7%) and aseptic loosening (16.5%) (Canadian Institute for Health Information, 2018). The bone cement routinely used in rTKA is poly(methyl methacrylate) (PMMA) (Cawley, Kelly, McGarry, & Shannon, 2013; Fehring, Odum, Calton, & Mason, 2000; Stevens, Tetsworth, Calhoun, & Mader, 2005). PMMA primarily acts as a grout, only adhering mechanically to the surface with little-to-no chemical interaction with bone (Skripitz & Aspenberg, 1999; Vaishya, Chauhan, & Vaish, 2013), and has poor osteointegration (Buchanan, 2019). Moreover, PMMA

has side-effects such as thermal necrosis due to heat generation during the polymerization process, aseptic loosening (Abu-Amer, Darwech, & Clohisy, 2007), wear debris (Horowitz, Gautsch, Frondoza, & Riley, 1991; Jiang, Jia, Gong, Wooley, & Yang, 2013), and volumetric shrinkage (Haas, Brauer, & Dickson, 1975). These can lead to failure at the bone-PMMA interface and subsequent bone loss (Birkeland, Espehaug, Havelin, & Furnes, 2017). Currently, the application of PMMA in rTKA is limited to minor peripheral bone defects which have a depth less than 5 mm and cover under 50% of the bone surface (Fosco, Ayad, Amendola, & Tigani, 2012; Qiu, Yan, Chiu, & Ng, 2012).

$CaSO_4$ has long been used for filling bone cavities in orthopedics (Kumar, Nalini, Menon, Patro, & Banerji, 2013; Peltier, Bickel, Lillo, & Thein, 1957; Thomas & Puleo, 2009; Thomas, Puleo, & Al-Sabbagh, 2005). In 1953, $CaSO_4$ pellets were used to fill defects in the tibial shaft which showed promising results: primary healing of the wounds, gradual absorption of $CaSO_4$, and finally bone regeneration (Peltier et al., 1957). The literature has reported properties such as biodegradability, osteoconductivity, and biocompatibility for $CaSO_4$ (Huan & Chang, 2007; Lazáry et al., 2007; Peltier et al., 1957; Sidqui, Collin, Vitte, & Forest, 1995). Fast resorption rate for $CaSO_4$ bone graft substitute has also been reported (Kuo et al., 2012; Thomas et al., 2005). Therefore, in this study, resorbable $CaSO_4$ ($CaSO_4 \cdot 0.5H_2O$) was incorporated to increase the porosity of GPC and bone formation through the pores. New bone formation requires bone graft substitutes with pore diameters greater than 100 μm to facilitate bone growth and pore diameters less than 10 μm to increase fluid diffusion (Kuo et al., 2012). Moreover, another rationale for addition of $CaSO_4$ was to increases the bioactivity of GPC by providing more Ca^{2+} ion which plays an essential role in bone formation and maturation (Orellana, Hilt, & Puleo, 2015). After dissolving in water, the concentration of calcium ions (Ca^{2+}) increases and this can stimulate osteoclast differentiation. Osteoclasts (large multinucleate bone cells that absorb bone tissue during growth and healing) have a calcium-sensing receptor and it is postulated that up to 40 mM of calcium would regulate the activity of osteoclast bone resorption through the calcium-sensing receptor(s) on the osteoclast cell membrane (Kameda et al., 1998).

Glass polyalkenoate cements (GPCs) were first introduced in 1972 as dental restorative materials (Alhalawani, Curran, Boyd, & Towler, 2016). GPCs are glass-based cements with an acid–base curing reaction (Walls, McCabe, & Murray, 1988). Low cytotoxicity, thermal compatibility with tooth structure and biocompatibility has resulted in extensive use of GPCs in dental applications as luting, lining and filling materials (Khoroushi & Keshani, 2013). GPCs do not set with an exothermic reaction and exhibit no significant volumetric shrinkage (Alhalawani et al., 2016). Commercial GPCs for dental restoration, such as Fuji IX GP (GC Europe NV, Leuven, Belgium) and Ketac Cem Easymix (3M ESPE, St. Paul, MN) contain aluminum ions (Al^{3+}) (Kim, Kim, Kim, & Kwon, 2011) that may cause defective bone mineralization (Blades, Moore, Revell, & Hill, 1998; Taïr et al., 2016). To address this issue, the chemistry of GPCs have been modified (Boyd, Clarkin, Wren, & Towler, 2008; Clarkin, Wren, Thornton, Cooney, & Towler, 2011), with elements such as zinc (Zn), strontium (Sr) and tantalum (Ta) added to Al-free GPCs in an attempt to avoid defective mineralization and impart antibacterial efficiency, biocompatibility, chemical stability and bone regeneration (Alhalawani, Mehrvar, Stone, Waldman, & Towler, 2017; Alhalawani & Towler, 2017; Boyd, Li, Tanner, Towler, & Wall, 2006; Clarkin et al., 2011). The GPC has been shown to bond chemically with bone due to ion exchange at the interface with the mineral phase of bone and the GPC (Khader, Peel, & Towler, 2017). Therefore, the purpose of this study was to modify a proprietary Al-free GPC (Alhalawani & Towler, 2017) by incorporating calcium sulfate ($CaSO_4$) in order to improve its bioactivity. The work herein investigates the chemical and mechanical properties of $CaSO_4$-containing GPCs as a bone void filler which may address current issues around the use of PMMA in rTKA.

2 | MATERIALS AND METHODS

2.1 | Glass synthesis

Previously, a series of aluminum-free bioactive glass systems containing no TA_2O_5 (SiO_2-ZnO-CaO-SrO-P_2O_5) namely TA_0, and two bioactive glass systems containing TA_2O_5 (SiO_2-ZnO-CaO-SrO-P_2O_5-X TA_2O_5) with x varying from x = 0.2 for TA_1 and x = 0.5 for TA_2 were fabricated in our group and mechanical and biological properties of these particular bioactive glass systems were investigated (Alhalawani & Towler, 2017). The result showed an increase in ion release and long-term mechanical properties in TA_2 glass system compared to TA_1 and TA_0. Moreover, the bioactive glass systems showed strong antibacterial and antifungal activity against both Gram-negative and Gram-positive bacteria. Cytotoxicity results indicated that the resultant GPC is non-toxic to cells (Alhalawani et al., 2017; Alhalawani & Towler, 2017). The bioactive glass used for this study was prepared by a glass manufacturer (Mo-Sci, Rolla, MO) using specified fraction (Table 1) according to the paper published by Alhalawani and Towler (2017). The resultant glass was sieved to <20 μm (Ishikawa, Matsuya, Miyamoto, & Kawate, 2007) to tailor the material for a suitable setting time for rTKA.

2.2 | Cement preparation

The initial GPCs were manufactured by mixing poly(acrylic acid) (PAA, Mw: ~50,000 and median particle size <90 μm, Sigma-Aldrich, St. Louis, MI), with appropriate amounts of glass powder and deionized (DI) water by using a metal spatula. The liquid to powder ratios were changed such that the cements' working and setting times vary within a suitable range for rTKA applications (P. Zalzal, personal communication, June 17, 2017) (Table 1). The powder to liquid ratio (P: L) was 1:1.5 (Table 1). Alongside a control series of GPCs that were free of $CaSO_4$, 1, 5 and 15 wt% of calcium sulfate hemihydrates ($CaSO_4 \cdot 0.5H_2O$, Sigma Aldrich, St. Louis, MO) with particle size of ~1.48 μm diameter were added to the GPC mixture. The modified cement is referred to as mGPC.

TABLE 1 Glass and cement composition and formulation

Glass formulations	SiO_2	ZnO	CaO	SrO	P_2O_5	Ta_2O_5	Cement formulation (glass(g): PAA(g): DI water)
Glass (wt%)	38.75	38.81	4.52	11.14	3.81	2.97	1 g:0.75 g:0.75 ml

2.3 | Working and setting times

The working time of the mGPCs (the time from the start of mixing until cement was able to manipulate) (ISO 9917-1:2007; 2007), was measured in ambient air (23 ± 1°C) with stopwatch. The setting time was measured in accordance with ISO 9917-1:2007 for dental based cements (ISO 9917-1:2007; 2007). An empty mold (10 mm × 8 mm × 5 mm) was placed on aluminum foil and filled with mixed cement. Sixty seconds after mixing commenced, the entire assembly was placed on a metal block (8 mm × 75 mm × 100 mm) in an oven maintained at 37°C. Ninety seconds after mixing, a 400 g needle indenter was lowered on the surface of the GPC (25°C). The needle remained on the surface for 5 s, the indent it made was observed and the process then repeated every 30 s until the needle failed to make a complete indent when observed at ×2 magnification. The net setting times of the five tests were recorded.

2.4 | Determination of compressive strength

The compressive strength (σ_c) of the mGPCs (n = 5, 6 mm high, 2 mm diameter) was tested according to ISO 9917-1:2007 for dental based cements (ISO 9917-1:2007; 2007). Each sample was prepared based on the addition of $CaSO_4$ (1, 5, and 15 wt% by mass of GPC), and aged in DI water for 1, 7, 14 and 30 days at 37°C. The samples were loaded on a United Universal Tester (STM-50KN, United Testing Systems, Inc., Huntington Beach, CA) using a 5 kN load cell at a crosshead speed of 1 mm/min. Compressive strength (GPa) was calculated using Equation (1):

$$C = \frac{4\rho}{\pi d^2} \quad (1)$$

where ρ was the maximum applied load (kN) at failure and d the sample diameter (mm). Moreover, the compressive strength of cast $CaSO_4$ (n = 5, 6 mm high, 2 mm diameter) was determined according to the above equation.

2.5 | Determination of biaxial flexural strength

The biaxial flexural strength (BFS) (σ_f) of the mGPCs (n = 5) was tested using a method described by Williams, Billington, and Pearson (2002). Cement discs (12 mm diameter, 2 mm thick) were tested after being aged for 1, 7, 14 and 30 days in DI water in a 37°C incubator. Testing was undertaken on a United Universal Tester (STM-50KN, United Testing Systems, Inc., Huntington Beach, CA) using a 5 kN load cell at a crosshead speed of 1 mm/min. The fracture strength was noted for each sample.

2.6 | Evaluation of ion release and pH

2.6.1 | Sample preparation

mGPC cylinders (6 mm high, 2 mm diameter) were prepared for pH testing and ion release studies. Solutions were prepared by incubating cylindrical samples (n = 5) in 10 ml of DI water at 37°C for 1, 7, 14 and 30 days. Changes in the pH of mGPC solutions were measured using a Corning 430 pH meter (n = 5). The pH meter was calibrated using two pH buffer solutions before testing; 4.00 ± 0.02 and 7.00 ± 0.02 (Fisher Scientific, Pittsburgh, PA). The ion release profile of each mGPC specimen was measured by atomic absorption spectroscopy (AAS) with a Perkin-Elmer Analyst 800 (Perkin Elmer, MA). AAS calibration standards for Ca, SO_4 and Zn elements were prepared from a stock solution. Calibration standards (0.5, 1, 2.5, 5 and 10 ppm) were prepared for each ion and DI water was used as a control.

2.7 | Scanning electron microscopy and energy dispersive X-ray analysis

Cross-sectional images from the mGPC samples (prepared according to Section 2.6) were taken using a JEOL Co. JSM-6380LV (JEOL Ltd., Tokyo, Japan) Scanning Electron Microscope. An EDX Genesis Energy-Dispersive Spectrometer (JEOL Co. JSM-6380LV, JEOL Ltd.) was used for compositional analysis.

2.8 | Fourier transform infrared spectroscopic study

mGPC cylinders (6 mm long, 4 mm diameter) of the unmodified Control and 1, 5 and 15 wt% $CaSO_4$ addition were prepared and aged for 1 and 30 days in DI water. ~0.3 g powdered versions (<90 μm) of each specimen were spread onto NaCl crystal discs (25 mm diameter). Spectra were collected using a Fourier transform infrared (FTIR) spectrometer (Spectrum One FTIR spectrometer, Perkin Elmer Instruments) and background contributions were removed. The sample and the reference background spectra were collected 16 times for each cement formulation in ambient air (23 ± 1°C). The analysis was performed in the wavenumber ranging from 900 to 4,000 cm^{-1} with a spectral resolution of 4 cm^{-1}.

2.9 | Micro-CT analysis

The structure of the mGPC was analyzed using a MicroCT (Locus Explore Scanner, GE Healthcare). The samples were incubated in DI

water for 30 days. An initial scan was performed, giving an overall X-ray image from which, an area of focus was then selected for scanning at full resolution (27 μm). Images were reconstructed and isosurfaced with selective thresholds.

2.10 | Porosity and density measurements of mGPC

The solvent replacement method was used for determination of porosity (Nanda, Sood, Reddy, & Markandeywar, 2013). mGPCs were aged in DI water for 24 hr. Next, the samples were weighed after excess water on the surface was blotted. Porosity was calculated from Equation (2).

$$P = (W_2 - W_1/\rho_{water} \times V) \times 100 \quad (2)$$

where W_1 is the mass of mGPC before immersion in DI water and W_2 is the mass of mGPC after immersion in DI water and V is the volume of mGPC cylinder. Moreover, the density of each specimen was measured by dividing W_1 over V.

2.11 | Statistical analysis

One-way analysis of variance (ANOVA) and Tukey's post-hoc test were used to statistically analyze the mean differences across the gathered data using Minitab 17 (Minitab Inc., State College, PA). Significance was associated with $p < .05$.

3 | RESULTS

3.1 | Working and setting times

Figure 1 shows the working time (t_w) and setting time (t_s) of the mGPC series. Pre-clinical feedback confirmed that a setting time of around 4–12 min was enough to apply the cement and insert a prosthesis (P. Zalzal, personal communication, June 17, 2017). Working times were recorded as 1.5 ± 0.16, 2.2 ± 0.13, 1.1 ± 0.08 and 1.7 ± 0.33 min for Control, 1, 5 and 15 wt% $CaSO_4$ addition, respectively (Figure 1). Table 2 shows that there were significant differences

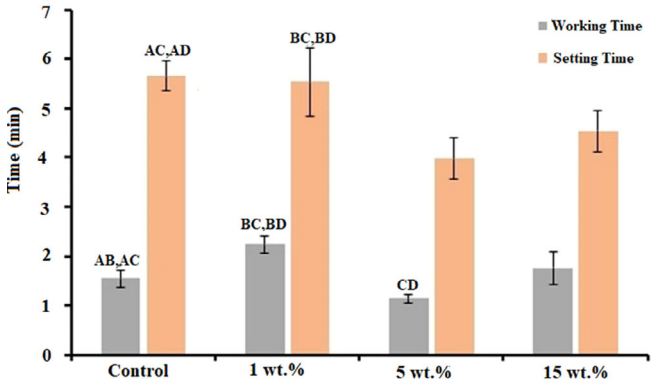

FIGURE 1 Working and setting times for Control, 1, 5 and 15 wt % of $CaSO_4$-mGPC. Error bars represent the. *SD* (n = 5). (a), (b), (c), and (d) denote statistically significant difference at $p \leq .05$ between. Control, 1, 5 and 15 wt% $CaSO_4$ addition

TABLE 2 The p value for working and setting time measurements with respect to the addition of $CASO_4$ according to ANOVA test

Means compared	p value (working time)	p value (setting time)
Control–1 wt%	$p < .001$	.977
Control–5 wt%	.033	$p < .001$
Control–15 wt%	.385	.009
1–5 wt%	$p < .001$	.001
1–15 wt%	.011	.021
5–15 wt%	.001	.297

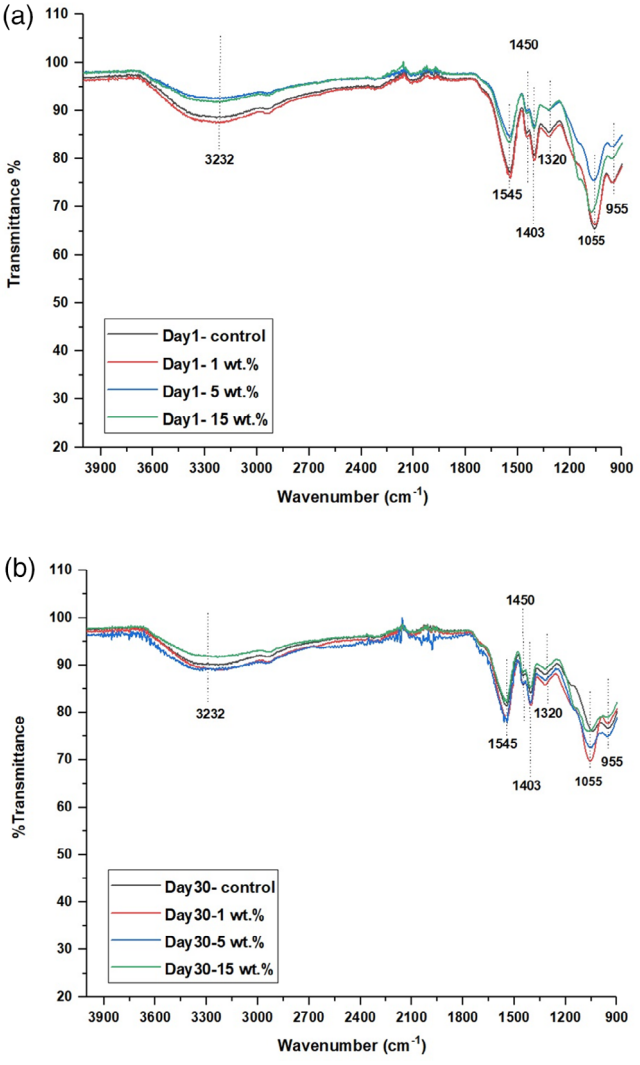

FIGURE 2 (a) FTIR spectra of cement series after 1 day maturation in DI water. (b) FTIR spectra of cement series after 30 days of maturation in DI water. DI, deionized; FTIR, Fourier transform infrared

in setting time between Control versus 5 wt%, Control versus 15 wt %, 1 versus 5 wt% and 1 versus 15 wt%. The GPC with 5 wt% $CaSO_4$ addition showed the shortest working (1.1 ± 0.08 min) and setting (3.9 ± 0.41 min) times (Figure 1).

3.2 | FTIR spectroscopic study

The FTIR spectroscopy of the cement series after immersion in DI water for 1 and 30 days is illustrated in Figure 2a,b. FTIR spectroscopy was conducted on Day 1 and Day 30 following maturation of mGPC in DI water to determine the reaction kinetics between the GPC and $CaSO_4$. Results were obtained in the range of 4,000–900 cm^{-1}. The resultant bands were centered at around 3,232, 1,545, 1,450, 1,403, 1,320, 1,055 and 955 cm^{-1}. FTIR results also showed the broad peak at 3,232 cm^{-1} for all spectra in Day 1 and Day 30 which is assigned to the O-H stretch of the absorbed water (Driessen, Miller, & Grassian, 1998).The peaks from 1,545 to 1,320 cm^{-1} are assigned to symmetric/asymmetric stretching vibrations of carboxyl COO^- which indicates the bounded COO^--X molecule (X represents a metal cation) (Alhalawani, Curran, Pingguan-Murphy, Boyd, & Towler, 2013; Crisp, Pringuer, Wardleworth, & Wilson, 1974). Moreover, the 1,055 cm^{-1} peak represents the Si-O-Si bridges of the GPC and the shoulder peak at 955 cm^{-1} is assigned to Si-OH deformation vibration (Matsuya, Maeda, & Ohta, 1996).

3.3 | SEM-EDS and micro-CT results

Scanning electron microscopy (SEM) was employed to produce images of the mGPC surface's topography (Figures 3 and 5), while energy dispersive x-ray spectroscopy (EDS) analysis was performed to provide the quantitative elemental analysis (wt%) of the mGPC series from the

TABLE 3 EDS result for each mGPC (a) Control, (b) 1 wt%, (c) 5 wt% and (d) 15 wt% $CaSO_4$ addition after 30 days maturation in DI water

Elements (wt%)	Control	1 wt%	5 wt%	15 wt%
Ca	2.4 ± 0.1	2.6 ± 0.2	3.4 ± 0.2	6.3 ± 0.1
Zn	22.3 ± 0.5	14.7 ± 0.6	20.5 ± 0.6	20.5 ± 0.7
S	—	0.4 ± 0.1	0.5 ± 0.1	0.6 ± 0.1

Note: wt% is related to amount of elements in the selected SEM (500 μm) area (average of 5 measurements).
Abbreviations: DI, deionized; EDS, energy dispersive x-ray spectroscopy.

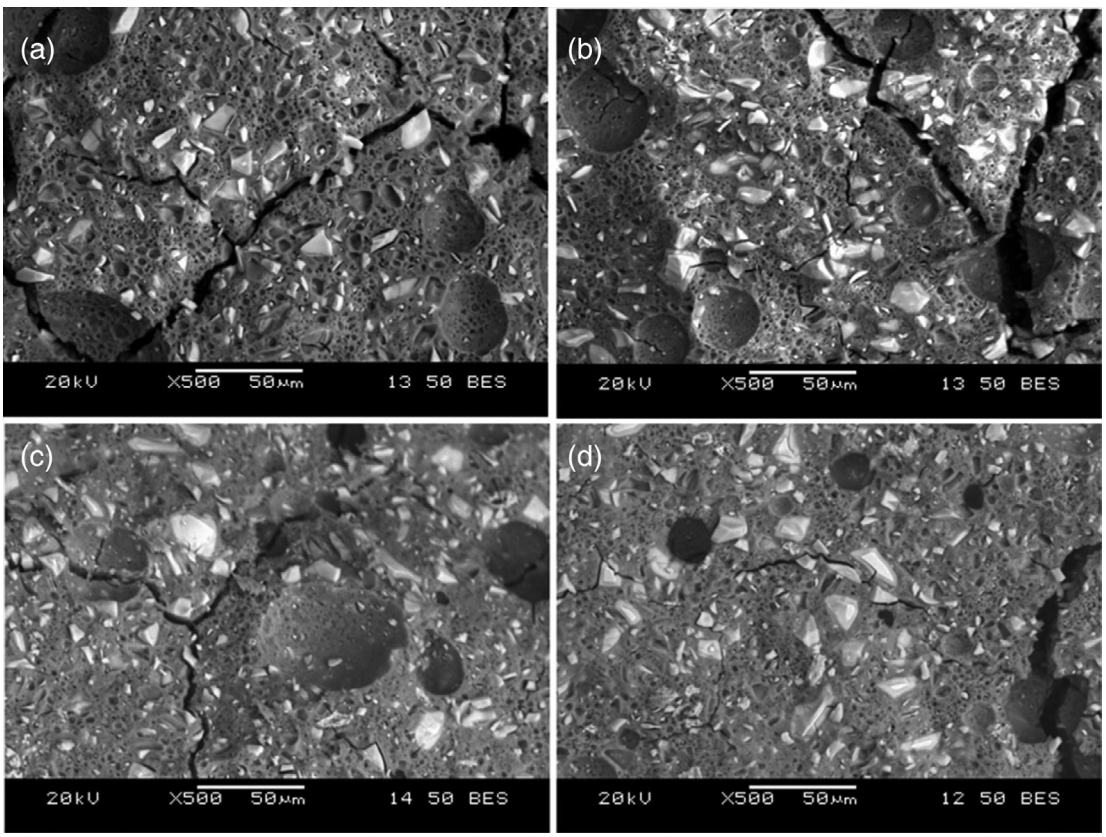

FIGURE 3 Backscattered SEM images from cross-section of each mGPC (a) Control, (b) 1 wt%, (c) 5 wt% and (d) 15 wt% $CaSO_4$ addition after 30 days maturation in DI water. DI, deionized; SEM, scanning electron microscopy

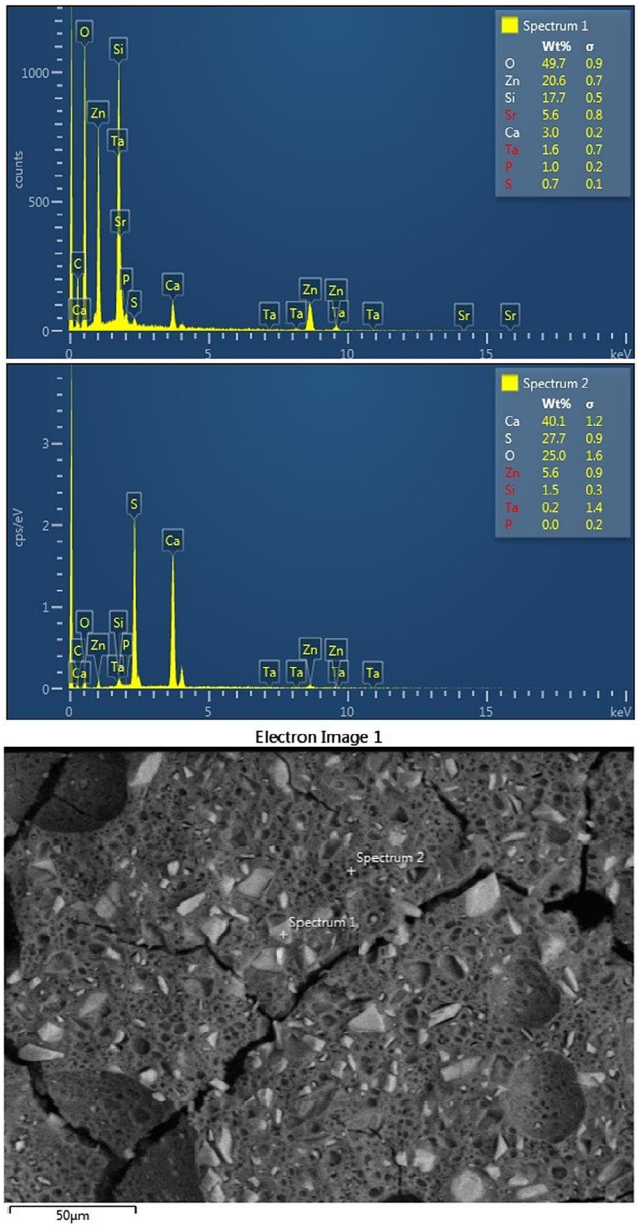

FIGURE 4 SEM-EDS analysis of 15 wt% $CaSO_4$ after 30 days maturation in DI water. DI, deionized; SEM-EDS, scanning electron microscopy-energy dispersive X-ray spectroscopy

SEM backscattered images (Table 3). Figure 3 shows cross-sectional SEM images from mGPC after 30 days of maturation in DI water. It confirmed the existence of micro-cracks and a random pore distribution with small (≤10 μm) and large pores (largely <50 μm) throughout the specimens. Small bright spots can be seen embedded in the polysalt matrix (Figure 3). Generally, the glass has a higher average atomic number than the acid component of polysalt, and therefore the unreacted glass particles appear brighter. Moreover, as can be seen in Figure 4, spectrum 2 shows an area of GPC which contained intact $CaSO_4$. Particle size analysis with Clemex Vision Image Analyzer (Clemex, Longueuil, Canada) confirmed that the $CaSO_4$ particles have ~1.48 μm diameter. Therefore, the large pores which are evident throughout the samples are most likely air bubbles formed due to hand mixing (Khader et al., 2017). Additionally, Figure 5 represents surface SEM images from mGPC after 30 day maturation in DI water. Control specimens showed larger and less frequent pores compared to other specimens. The pore size of mGPC specimens (~ 2 μm) at the surface (Figure 5) matches with $CaSO_4$ particle size (~ 1.48 μm). Therefore, it seems that the porous structure observed in the 1, 5 and 15 wt% $CaSO_4$ addition is evidence of $CaSO_4$ dissolving from the surface of mGPCs (Figure 5).

Figure 6a,b show the Micro-CT reconstruction (2D and 3D) of the mGPC series (Control and 15 wt% $CaSO_4$ addition). The porosity of mGPC does not appear to be changed significantly by increased $CaSO_4$ content. However, micropores with a diameter smaller than 20 μm were unlikely to be detected by Micro-CT (Cox, Wilcox, Levesley, & Hall, 2006).

3.4 | Porosity and density measurement results

The porosity (%) of mGPC specimens was obtained as shown in Figure 7. It was observed that $CaSO_4$ addition did not increase the porosity of mGPC significantly (Table 4). However, density showed no significant differences between Control, 1 and 5 wt% $CaSO_4$ addition (Table 5).

3.5 | pH study

Figure 8 represents the changes of pH value in mGPC series when aged in DI water for 30 days. There were significant decreases from 7.0 ± 0.11 to 6.1 ± 0.19 from Control to 15 wt% (p = .007) at Day 1. The same trend observed for Control versus 15 wt%, (p = .012) and 1 versus 15 wt% (p = .005) continued until Day 4. However, from Day 14, statistically significant differences were observed for Control versus 5 wt% (p = .038), Control versus 15 wt% (p = .002) and 1 versus 15 wt% (p = .003) and a similar trend (Control vs. 15 wt% [p = .002], and 1 vs. 15 wt% [p = .003]) was observed for Day 30. Therefore, it can be concluded that the addition of $CaSO_4$ decreased pH.

3.6 | Ion release profiles

Figures 9–11 represent the ion release profiles of Ca^{2+}, Zn^{2+}, and SO_4^{2-} over 1, 4, 7, 14 and 30 days maturation in DI water, respectively.

3.6.1 | Release of Ca^{2+}

As can be seen in Figure 9, the release of Ca^{2+} increased with the addition of $CaSO_4$. The release of Ca^{2+} increased significantly from 2 ppm for Control samples to 54 ppm for 15 wt% $CaSO_4$ addition (p = .000) on Day 1. This trend continued for Days 4 and 7. On Day

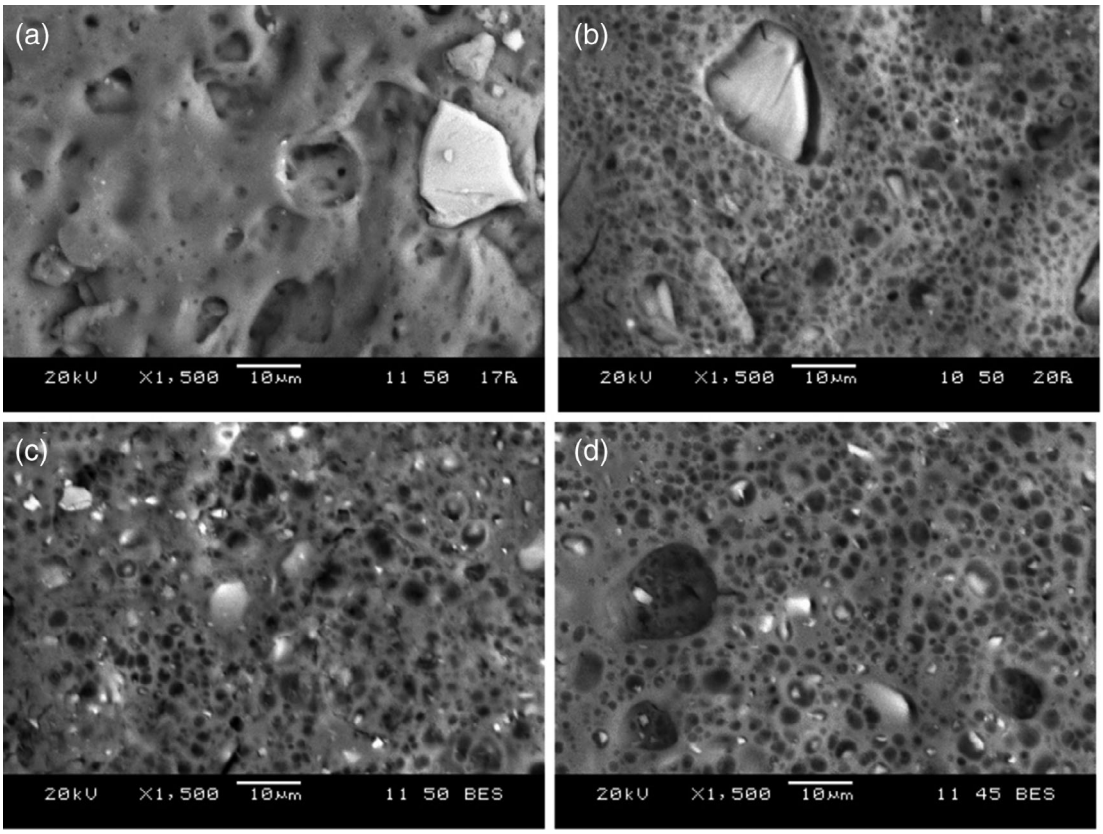

FIGURE 5 Backscattered SEM images from the surface of each mGPC (a) Control, (b) 1 wt%, (c) 5 wt% and. (d) 15 wt% $CaSO_4$ addition after 30 days maturation in DI water. DI, deionized; SEM, scanning electron microscopy

14, there was a burst release of Ca^{2+} (120 ppm and 155 ppm for 5 and 15 wt%, respectively). Although Ca^{2+} release for 5 wt% specimens showed no significant differences from Day 14 to Day 30, the release for 15 wt% $CaSO_4$ addition decreased significantly between Day 14 and Day 30. The maximum release of Ca^{2+} ions on Day 30 was reported as 124 ppm.

3.6.2 | Release of Zn^{2+}

The release of Zn^{2+} has been demonstrated in Figure 10. There was a significant difference between Control versus 15 wt% (p = .015) and 1 versus 15 wt% (p = .028) for Day 1. No significant differences were found for Day 4 and Day 14 among all specimens, but release measurements of Zn^{2+} on Day 7 (Control vs. 15 wt% [p = .004], 1 vs. 15 wt% [p = .026] and 5 vs. 15 wt% [p = .016]) and on Day 30 (1 vs. 5 wt% [p = .002], 1 vs. 15 wt% (p = .024), Control vs. 5 wt% [p = .002], Control vs. 15 wt% [p = .024]) were significantly different.

3.6.3 | Release of SO_4^{2-}

Figure 11 displayed the SO_4^{2-} release over 30 days ageing in DI water. Similar to Ca^{2+}, the release profile of SO_4^{2-} showed an increasing trend with addition of $CaSO_4$ which was dependent on maturation time. Day 1 results showed significant differences for 1 versus 15 wt% and 5 versus 15 wt% at p = .001. This trend continued for Day 4 (1 vs. 15 wt% p = .008 and 5 vs. 15 wt% p = .001) and Day 7 (5 vs.15 wt% p < .001 and 1 vs. 15 wt% p = .002). The statistical analysis showed significant differences with regards to 5 wt% $CaSO_4$ addition for Day 1 versus Day 30 (p = .003), Day 4 versus Day 30 (p = .008) and Day 7 versus Day 30 (p = .010). For 15 wt% samples, the only significant difference was for Day 1 versus Day 14 with p = .030.

3.7 | Mechanical properties evaluation

3.7.1 | Determination of compressive strength

The compressive strengths (σ_c) of the cement series after 1, 4, 7 and 30 days maturation in DI water are presented in Figure 12. The compressive strength was influenced by two factors, maturation time and the amount of $CaSO_4$ incorporated into the GPC. There was a significant difference in Control versus 5 wt% (p = .001) and Control versus 15 wt% (p = .002) at Day 1. Since the 5 and 15 wt% mGPC showed the shortest setting time (Figure 1) among all the groups, it was assumed that they would have higher initial strength. As expected, no

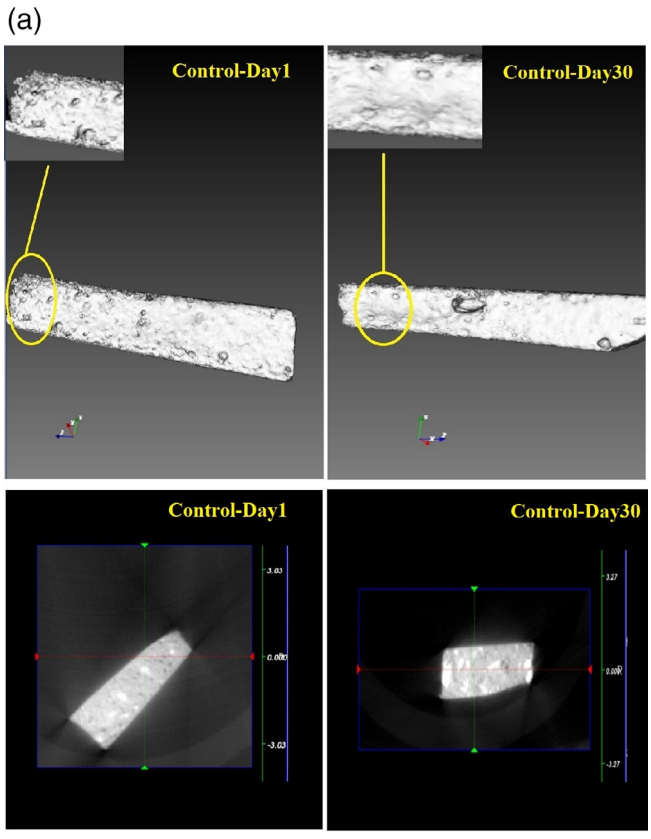

FIGURE 6 (a) 3D and 2D reconstruction from the cross-section of control samples provided by Micro-CT on Day 1 and Day 30. Angle (x, y, z): 90.0°, 180.0°, 90.0. (b) 3D and 2 D reconstruction from the cross-section of 15wt% samples provided by Micro-CT on Day 1 and Day 30. Angle (x, y, z): 90.0°, 180.0°, 90.0

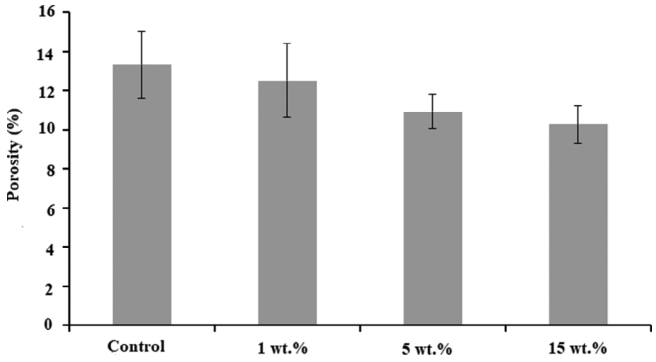

FIGURE 7 Porosity (%) of mGPCs after 1 day immersion in DI water. DI, deionized

TABLE 4 The *p* value for porosity measurements with respect to the addition of $CaSO_4$ according to ANOVA test

Means compared	*p* value
Control–1 wt%	.898
Control–5 wt%	.245
Control–15 wt%	.112
1–5 wt%	.552
1–15 wt%	.286
5–15 wt%	.937

significant difference was observed among all groups after aged for 14 days in DI water.

3.7.2 | Determination of BFS

The BFS of the cement series at 1, 4, 7, 14 and 30 days is presented in Figure 13. The highest σ_f was 12.5 ± 1.7 MPa, obtained for 5 wt% $CaSO_4$ addition after 7 days maturation. There was no significant difference in σ_f with respect to maturation time for Day 1 and Day 4. There was a significant increase in Control versus 5 wt%, (p = .01) and Control versus 15 wt% (p = .017) on Day 7, but no significant differences were observed for Control versus 5 wt% and Control versus 15 wt% on Day 14 and Day 30. The incorporation of $CaSO_4$ into GPC showed the following trends with respect to BFS measurement; (a) control: no significant differences over 30 days. (b) 1 wt% $CaSO_4$ addition: a significant difference for Day 1 versus Day 7 (p = .029). (c) 5 and 15 wt% $CaSO_4$ addition: no significant differences over 30 days.

4 | DISCUSSION

The mGPC specimens were produced as a result of mixing the reagents (according to Section 2.2) and then working times and

TABLE 5 Average density of mGPC specimens (g/cm^3)

Control	1 wt%	5 wt%	15 wt%
1.29 ± 0.11	1.31 ± 0.08	1.35 ± 0.13	1.52 ± 0.12

setting times of mGPC series were evaluated with respect to increasing $CaSO_4$ content. Furthermore, FTIR spectroscopy was used to provide characteristic information on the setting reaction of mGPC. The 1 wt% $CaSO_4$ addition resulted in GPCs with the longest working

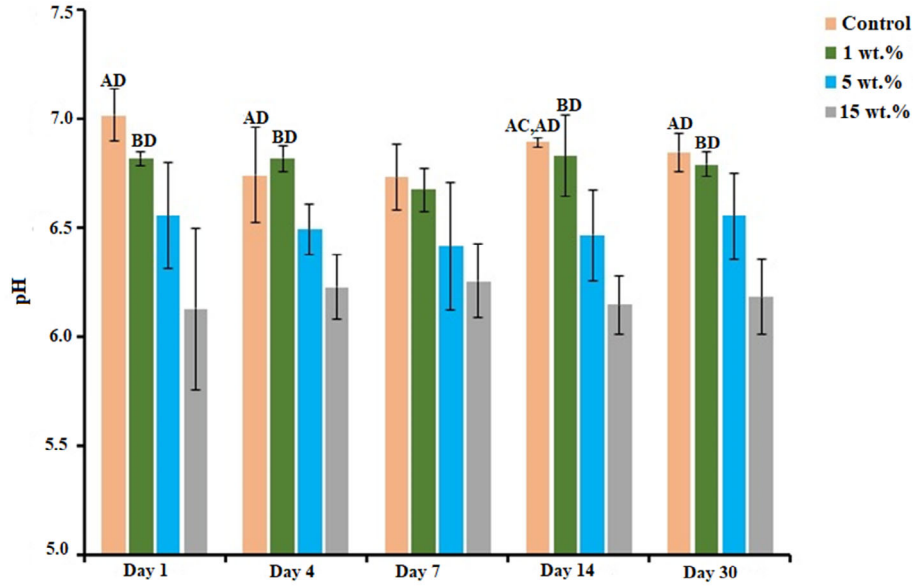

FIGURE 8 pH measurements of the cement maturation solutions in DI water for 1,7,14 and 30 days, post cement preparation. Error bars represent *SD* (n = 5). (a), (b), (c) and (d) denote statistically. significant difference at $p \leq .05$ between Control,1, 5 and 15 wt% $CaSO_4$ addition. DI, deionized

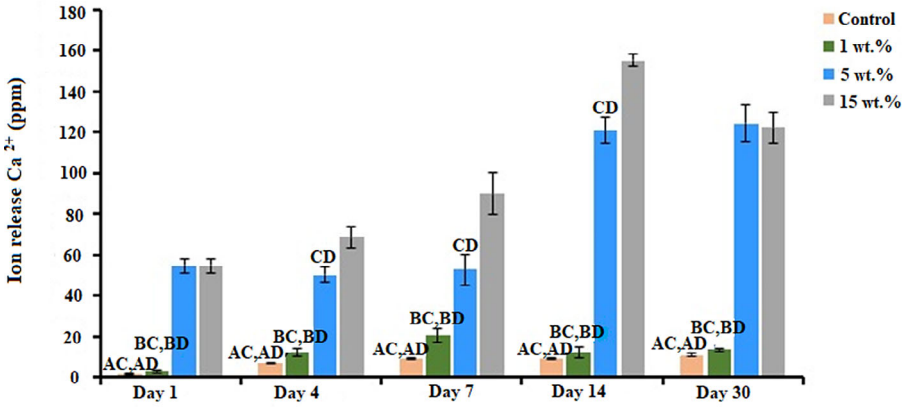

FIGURE 9 Release profiles of Ca^{2+} ions during cement aging in DI water. Error bars represent *SD* (n = 5). (a), (b), (c), and (d) denote statistically significant difference at $p \leq .05$ between. Control, 1, 5 and 15 wt% $CaSO_4$ addition. DI, deionized

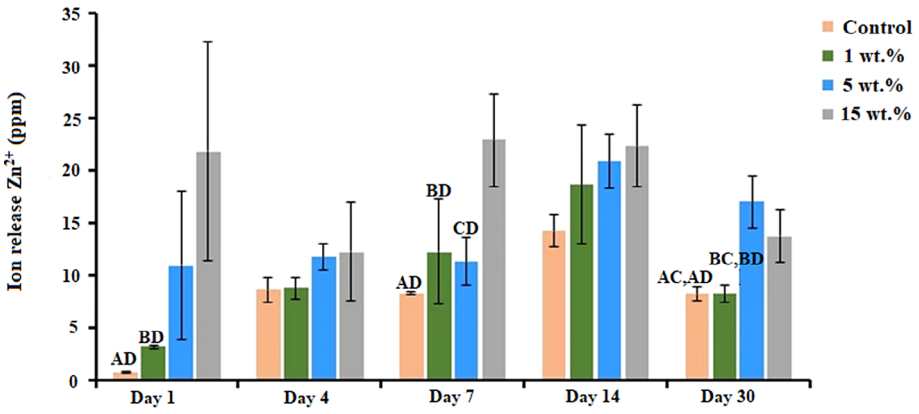

FIGURE 10 Release profiles of (a) Zn^{2+} ions during cement aging in DI water. Error bars represent *SD* (n = 5). (a), (b), (c), and (d) denote statistically significant difference at $p \leq .05$ between. Control, 1, 5 and 15 wt% $CaSO_4$ addition. DI, deionized

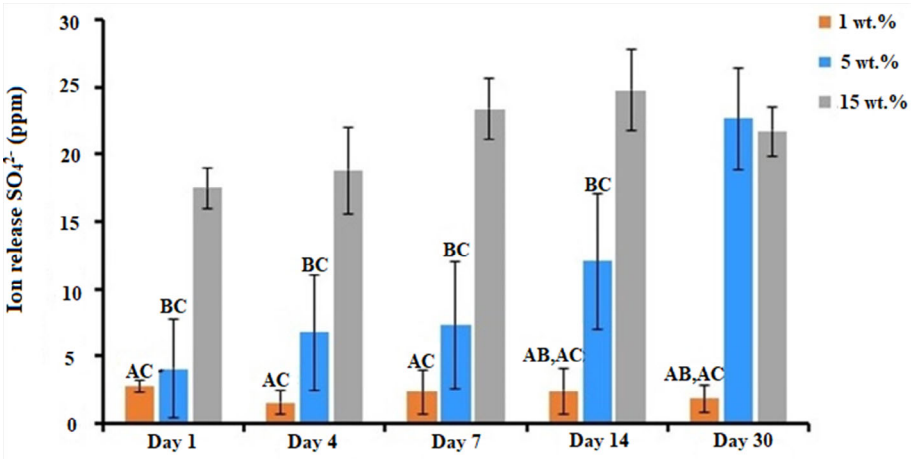

FIGURE 11 Release profiles of SO_4^{2-} ions during cement aging in DI water. Error bars represent *SD* (n = 5). (a), (b), (c), and (d) denote statistically significant difference at $p \leq .05$ between. Control, 1, 5 and 15 wt% $CaSO_4$ addition. DI, deionized

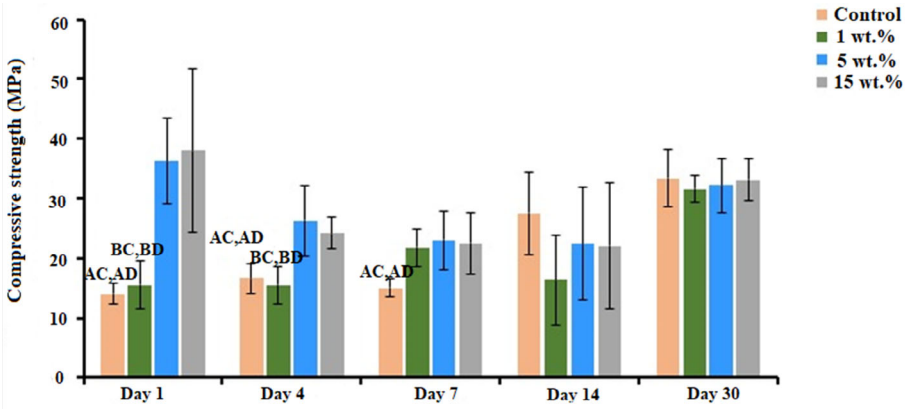

FIGURE 12 Compressive strengths of the GPC (Control) and GPC incorporated with 1, 5 and 15 wt% when aged in DI water for 1, 7 and 30 days. Error bars represent *SD* (n = 5). (a), (b), (c), and (d). denote statistically significant difference at $p \leq .05$ between Control, 1, 5 and 15 wt% $CaSO_4$ addition. DI, deionized

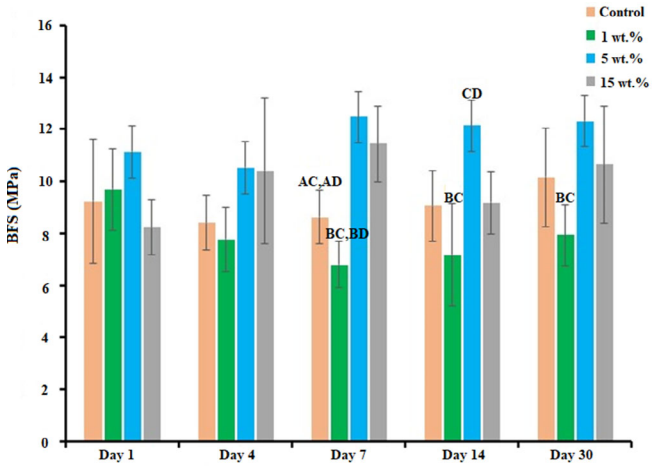

FIGURE 13 Biaxial flexural strength of the cement series when aged in DI water after 1, 7 and 30 days. Error bars represent *SD* (n = 5). (a), (b), (c), and (d) denote statistically significant difference at $p \leq .05$. between Control, 1, 5 and 15 wt% $CaSO_4$ addition. DI, deionized

times of all specimens. According to the FTIR study, 1 wt% $CaSO_4$ addition showed the most absorbed water among all specimens. Therefore, the longest working time might be related to the slower reaction of glass and PAA due to excess water. The shorter setting time for the 5 and 15 wt% $CaSO_4$ addition could be explained by FTIR results which indicated that the incorporation of 5 and 15 wt% $CaSO_4$ resulted in less absorbed water compared to Control and 1 wt%. Additionally, the setting time rate of the GPC was influenced by the P:L ratio. The shorter setting time in 5 and 15 wt% $CaSO_4$ addition might be attributed to an increased P:L ratio in comparison with Control and 1 wt% samples. Therefore, $CaSO_4$ particles might act in a similar fashion to unreacted glass particles in the polymeric matrix and decrease t_s (Khoroushi & Keshani, 2013; Nicholson, 2018).

FTIR results also showed a broad peak at 3232 cm^{-1} for all spectra which is assigned to the O-H stretch of the absorbed water (Driessen et al., 1998). Increasing the amount of $CaSO_4$ to 5 and 15 wt% resulted in less water absorption in comparison with both Control and 1% samples on Day 1. Moreover, according to Figure 2b, there was a decrease in water content for the 15 wt% $CaSO_4$ addition compared to other groups on Day 30. The peaks from 1,545 to 1,320 cm^{-1} indicate the bounded COO^--X molecule (X represents a metal cation) (Alhalawani et al., 2013; Crisp et al., 1974). Therefore, these peaks show the cross-linking of a dissociated COO^- group with a metal cation to form metal carboxylate. The setting of GPC is dependent on the cross-linking of COO^- and metal cations resulting in gelation of polycarboxylate and matrix formation. This process usually takes quite a few minutes to be completed (Walls, 1986). No change in frequency between Control and $CaSO_4$ incorporated

samples was observed at Day 1 and similar trend was observed for Day 30. Therefore, it can be concluded that most of $CaSO_4$ particles did not cross-link with COO^- as the wavenumber for both Day 1 and Day 30 remained unchanged. Overall, it can be concluded that $CaSO_4$ did not cross-link with the GPC. However, the incorporation of $CaSO_4$ reduced the amount of absorbed water within the poly-salt matrix for 5 and 15 wt% $CaSO_4$ addition specimens.

EDS results presented in Table 3 confirmed that the mGPC specimens contained Zn, Ca and sulfur (S). The incorporation of $CaSO_4$ increased the amount of Ca from 2.4 to 6.3 wt% through the series. Moreover, S content increased from 0.4 wt% at 1 wt% $CaSO_4$ addition and surged to 0.6 wt% at 15 wt% $CaSO_4$ addition. The incorporation of $CaSO_4$ was found to decrease the wt% of the Zn in the 1 wt% $CaSO_4$ addition which may explain the longer working time compared to other mGPC specimens. Zn acts as an intermediary in a glass structure (network modifier [ZnO_6] or network former [ZnO_4]) and increases the strength of the glass network (Alhalawani & Towler, 2016; Towler et al., 2006). Therefore, decreasing the amount of Zn could lead to an increase in working time. The amount of Zn increased for both 5 and 15 wt% $CaSO_4$ addition compared to 1 wt% specimens. The following assumptions could affect the accuracy of the EDS results:

1 In quantitative EDS analysis, the sample must be flat, polished and free of any voids (Newbury & Ritchie, 2015). Therefore, the porous structure of the GPC could affect the results.
2 EDS provides characterization at the surface depth of 2–5 μm. This could cause overlapping issues and discrepancies between elements (Alhalawani & Towler, 2017).

In general, the SEM micrographs verified the presence of pores among all specimens, while EDS results confirmed the presence of $CaSO_4$ at the cross-section of all $CaSO_4$-containing GPCs after 30 days maturation. Regardless of the $CaSO_4$ content. Further, it was found that porosity is only affected by dissolving particles at the surface and not within the mGPC specimen, therefore, overall porosity did not change significantly.

pH results showed that addition of $CaSO_4$ would decrease the pH of GPC. When GPC is aged in water, hydrogen atoms dissociate the structure of the polycarboxylic chains and glass particles release cations into the surrounding environment (Wasson & Nicholson, 1991). During the initial setting of GPC, acidic polymers attack Ca^{2+} ions first. This process depends on the concentration of the hydrogen ions on COOH groups in the GPC matrix (Wandelt, ; Woolford, 1989). Different factors affect the pH of mGPC. The water in GPC is the reaction medium and solvent for polyalkenoate acid. In this experiment, we added a certain amount of water (750 ml), acid (750 ml) and glass (1 g). while the $CaSO_4$ amount was increased from 1 to 15 wt%. This means that due to the high amount of $CaSO_4$ (some particles will dissolve, and some will remain intact in water), there will not be enough medium for acid to attack the glass cations, therefore, ionization and subsequently ion-exchange balance will be disturbed. The hydrogen bonds cannot be replaced by ionic bonds and a large number of carboxylic acid groups will cause a drop in pH. The literature reports that the release of Zn^{2+} increases under acidic conditions in bioactive glasses (Murphy, Boyd, Moane, & Bennett, 2009; Zheng et al., 2016). Therefore, higher release of Zn^{2+} for 15 wt% $CaSO_4$ addition could be related to decrease in pH. It has been reported that locally altered pH influences osteogenesis (Thomas & Puleo, 2009). More specifically, increased acidity which is related to the dissolution of $CaSO_4$ can cause localized demineralization, thereby liberating growth factors previously incorporated into the bone matrix (Thomas & Puleo, 2009).

One of the major restrictions in using PMMA for filling large bone defects is its lack of bioactivity (Frazer, Byron, Osborne, & West, 2005). GPC is considered a bioactive material as a result of releasing therapeutic ions into the surrounding environment. Most of the incorporated elements (e.g., Zn and Ca) have been added to the glass phase to increase its therapeutic benefits and stabilize the structure of the GPC. Zn is an essential element which is a co-factor for many enzymes and stimulates protein synthesis, resulting in osteoconductivity (Rabiee, Nazparvar, Azizian, Vashaee, & Tayebi, 2015). Moreover, increased calcium intake results in an increased bone mineral growth rate up to a certain level (1,000 mg/day for adults between 19 and 50 years old [Cashman, 2002; Ross et al., 2011]) and helps rebuild bone tissue. Ca^{2+} is also a potential regulator in wound healing (Winkler, Sass, Duda, & Schmidt-Bleek, 2018). Therefore, the effect of increasing $CaSO_4$ content and maturation time on the $Ca^{2+,}$ Zn^{2+}, and SO_4^{2-} release into the DI water was evaluated.

The release of Ca^{2+} increased with the addition of $CaSO_4$ for the first 14 days which followed by less ion release at Day 30. Basically, the maturation of GPC depends on ions chelating with acid chains to form set GPC. The Ca^{2+} ions measured here are those not involved with the reaction (i.e., those which not chelate with acid chain) and therefore released into the media. Moreover, another source for Ca^{2+} ion release was $CaSO_4$ particles which incorporated into the mGPC matrix. FTIR results indicated no increase in cross-linking with addition of $CaSO_4$ at Day 1 and Day 30. Therefore, some particles released into the media without a reaction. There is also probability that some $CaSO_4$ particles might precipitate.

The release of Zn^{2+} showed fluctuation. The reason for this fluctuation is unclear but might be related to the setting chemistry of the GPC. Setting chemistry of GPC is based on the acid–base reaction between glass and PAA (Nicholson, 1998). This reaction starts with acid attacking the glass cations such as Zn^{2+} (Alhalawani & Towler, 2016). Next, the released cations would cross-link the polyanion chains of the acid. The dissolution of $CaSO_4$ increases the acidity of the solution which allows more of these cations to leach out of the glass and bind with the charged polyacid chain. Therefore, after 30 days, stronger polymeric bonds can be expected between the acid and glass in 5 and 15 wt% $CaSO_4$ addition. This would lead to lower zinc diffusion and decreased ion release. Moreover, more Ca^{2+} ions released from 5 to 15 wt% samples might exchange with Zn^{2+} ions in the cross-linked mGPC and enter the solution. These would cause fluctuation in the ion release of Zn^{2+}. Overall, the ion release results

showed the accelerated release of Ca^{2+} and SO_4^{2-} over the first 14 days and it was significantly different than that of the Control. According to Figure 5, $CaSO_4$ was dissolved mostly from the surface of mGPCs. Therefore, it can be concluded that the increased ion release was due to an absence of cross-linking in the $CaSO_4$ and the GPC (i.e., $CaSO_4$ was a separate phase which did not react with the GPC).

Based on the compressive strength results, incorporation of $CaSO_4$ increases the strength at Day 1. Some composite materials follow a simple Rule of Mixtures (Equation 3) (Callister & Rethwisch, 2018), which can be used to estimate the strength of the composite, that is,

$$\sigma_{\text{composite}} = V_p\sigma_p + (1 - V_p)\,\sigma_m \tag{3}$$

$$Vp = V_{\text{CaSO}_4\text{ particle}} / \left(V_{\text{CaSO}_4\text{ particle}} + V_{\text{matrix}}\right) \tag{4}$$

where σ_m is matrix stress at the failure strain (obtained from the GPC compressive strength results), σ_p is the stress of $CaSO_4$ particles (obtained from the compressive strength result for $CaSO_4$ cast) and V_p is the effective volume fraction of the $CaSO_4$ particles (obtained from Equation (4) and Table 5). Table 6 shows that the results calculated from the rule of mixture are a good fit for the experimental results. Therefore, it can be concluded that addition of $CaSO_4$ to GPC matrix increases the initial compressive strength.

Overall, both the Control GPC and mGPC in the current study have significantly higher compressive strengths than cancellous bone (1.2–7.8 MPa [Hvid, Christensen, Søondergaard, Christensen, & Larsen, 1983]). This may be an important factor in managing bone loss under load-bearing conditions such as the knee. Although the initial compressive strength of the mGPC (~30 MPa) is lower than that of PMMA (~95 MPa) (Abouazza, Condon, Hannigan, & Dunne, 2016), the compressive strength of mGPC is closer to that of cancellous bone (~1.2–7.8 MPa) (Hvid et al., 1983) which decreases the effect of stress-shielding (Kim, An, Huh, & Kim, 2019).

The Control in the current study showed a higher maximum compressive strength at Day 30 (~30 MPa) compared with that in a similar study published by Alhalawani et al. (Alhalawani et al., 2017) (~18 MPa) using a similar glass composition and the same P:L ratio (TA2); likely due to the physicality of the glass phase (the glass particles in this study were sieved to ≤20 μm, whereas in (Alhalawani et al., 2017) they were ≤45 μm, the smaller particle size resulting in a greater surface area available for reaction, leading to a faster setting and increasing strength. From the BFS results, it can be concluded that the incorporation of $CaSO_4$ does not significantly affect BFS, but increases compressive strength. In biaxial flexural loading, strength is limited by the relatively lower failure stress in tension (compared to compression) experienced by one half of the cross-section of the cement. Therefore, the $CaSO_4$ particles might have a positive effect on the initial compressive strength, but they seem not to alter the tensile strength.

TABLE 6 Comparison of mGPC strength with two methods (rule of mixture vs. experiment) obtained on Day 1

Composite	Rule of mixture (MPa)	Experiment (MPa)
1 wt%	15.7	15.5
5 wt%	35.9	36.3
15 wt%	36.8	38.0

5 | CONCLUSIONS

PMMA bone cement is contra-indicated for large bone defects in rTKA. The rTKA market size was valued to be US $8.0 B in 2017 with a growth rate of 3.7%. However, PMMA is the only commercial bone cement on the market which is currently being used for bone void filling and implant fixation to the bone in rTKA. Drawbacks such as crack propagation, bone necrosis, and loosening restrict the application of PMMA to defects whose depth is less than 5 mm. This study is directed at developing an experimental cement as a possible alternative for PMMA in rTKA. In this study, the incorporation of $CaSO_4$ into Glass Polyalkenoate Cement (GPC) has been investigated. The pore size of $CaSO_4$ incorporated into mGPC was found to be less than 10 μm. Although pores less than 10 μm increase the fluid diffusion, bone formation requires bone graft substitutes with pore diameters greater than 100 μm to facilitate bone growth. Therefore, the resultant mGPC cannot be used for bone regeneration purposes due to small pore diameters. The shorter setting time of the 5 wt% group might have a positive effect by reducing operating costs with a fast-setting GPC. Incorporation of 5 and 15 wt% of $CaSO_4$ into the GPC increases the ion release of Ca^{2+} and Zn^{2+} ions (compared to Control) after 30 days of maturation in DI water. One of the issues with PMMA is its lack of bioactivity upon implantation. Therefore, the release of therapeutic ions would increase the anti-bacterial and anti-inflammatory properties of the modified GPC. Furthermore, another drawback of PMMA is the lack of osteointegration. The addition of $CaSO_4$ and bioactive glass resulted in the formation of pores near the surface, which would be expected to increase osteointegration. FTIR results prove that $CaSO_4$ is unable to cross-link with GPC and remains as a distinct phase. 5 and 15 wt% $CaSO_4$ addition show higher initial compressive strength (more than 30 MPa) compared to Control (13.98 MPa) and this trend continues for 7 days. However, the modified GPC does not improve the BFS significantly. Therefore, the strength of the modified GPC might be low to be used solely for bone defects greater than 5 mm in rTKA and therefore not suitable for load-bearing applications. The current research was focused on preliminary analysis of the chemical and mechanical properties of the modified GPC. Further research will assess the in vitro (anti-bacterial and cytotoxicity) testing to evaluate the potential of this material as an alternative to PMMA in the rTKA space.

ACKNOWLEDGMENT

The authors would like to thank CIHR/NSERC-Collaborative Health Research Projects (356780-DAN) for financial support.

REFERENCES

Abouazza, O. A., Condon, F., Hannigan, A., & Dunne, C. (2016). In vitro comparative assessment of the mechanical properties of PMMA cement and a GPC cement for vertebroplasty. *Journal of Orthopaedics*, *13*, 81–89.

Abu-Amer, Y., Darwech, I., & Clohisy, J. C. (2007). Aseptic loosening of total joint replacements: Mechanisms underlying osteolysis and potential therapies. *Arthritis Research & Therapy*, *9*, S6.

Alhalawani, A. M., Curran, D. J., Boyd, D., & Towler, M. R. (2016). The role of poly (acrylic acid) in conventional glass polyalkenoate cements. *Journal of Polymer Engineering*, *36*(3), 221–237.

Alhalawani, A. M., Mehrvar, C., Stone, W., Waldman, S. D., & Towler, M. R. (2017). A novel tantalum-containing bioglass. Part II. Development of a bioadhesive for sternal fixation and repair. *Materials Science & Engineering. C, Materials for Biological Applications*, *71*, 401–411.

Alhalawani, A. M. F., Curran, D. J., Pingguan-Murphy, B., Boyd, D., & Towler, M. R. (2013). A novel glass polyalkenoate cement for fixation and stabilisation of the ribcage, post sternotomy surgery: An ex-vivo study. *Journal of Functional Biomaterials*, *4*, 329–357.

Alhalawani, A. M. F., & Towler, M. R. (2016). The effect of ZnO↔Ta2O5 substitution on the structural and thermal properties of SiO2-ZnO-SrO-CaO-P2O5 glasses. *Materials Characterization*, *114*, 218–224.

Alhalawani, A. M. F., & Towler, M. R. (2017). A novel tantalum-containing bioglass. Part I. Structure and solubility. *Materials Science and Engineering: C*, *72*, 202–211.

Birkeland, Ø., Espehaug, B., Havelin, L. I., & Furnes, O. (2017). Bone cement product and failure in total knee arthroplasty. *Acta Orthopaedica*, *88*, 75–81.

Blades, M. C., Moore, D. P., Revell, P. A., & Hill, R. (1998). In vivo skeletal response and biomechanical assessment of two novel polyalkenoate cements following femoral implantation in the female New Zealand white rabbit. *Journal of Materials Science: Materials in Medicine*, *9*, 701–706.

Boyd, D., Clarkin, O. M., Wren, A. W., & Towler, M. R. (2008). Zinc-based glass polyalkenoate cements with improved setting times and mechanical properties. *Acta Biomaterialia*, *4*, 425–431.

Boyd, D., Li, H., Tanner, D. A., Towler, M. R., & Wall, J. G. (2006). The antibacterial effects of zinc ion migration from zinc-based glass polyalkenoate cements. *Journal of Materials Science: Materials in Medicine*, *17*, 489–494.

Buchanan, E. P. (2019). *Pediatric Craniofacial Surgery: State of the Craft, An Issue of Clinics in Plastic Surgery, E-Book*, 46, (pp. 174–180). United States: Elsevier Health Sciences.

Callister, W. D., & Rethwisch, D. G. (2018). Composites. *Materials science and engineering: An introduction*, , . New York: Wiley.

Canadian Institute for Health Information. (2018). *Hip and knee replacements in Canada, 2016–2017: Canadian Joint Replacement Registry Annual Report*. Ottawa, ON: CIHI.

Cashman, K. D. (2002). Calcium intake, calcium bioavailability and bone health. *The British Journal of Nutrition*, *87*(Suppl 2), S169–S177.

Cawley, D. T., Kelly, N., McGarry, J. P., & Shannon, F. J. (2013). Cementing techniques for the tibial component in primary total knee replacement. *The Bone & Joint Journal*, *95-B*, 295–300.

Clarkin, O., Wren, A., Thornton, R., Cooney, J., & Towler, M. (2011). Antibacterial analysis of a zincbased glass polyalkenoate cement. *Journal of Biomaterials Applications*, *26*(3), 277–292.

Cox, B. D., Wilcox, R. K., Levesley, M. C., & Hall, R. M. (2006). Assessment of a three-dimensional measurement technique for the porosity evaluation of PMMA bone cement. *Journal of Materials Science: Materials in Medicine*, *17*, 553–557.

Crisp, S., Pringuer, M. A., Wardleworth, D., & Wilson, A. D. (1974). Reactions in glass ionomer cements: II. An infrared spectroscopic study. *Journal of Dental Research*, *53*, 1414–1419.

Driessen, M. D., Miller, T. M., & Grassian, V. H. (1998). Photocatalytic oxidation of trichloroethylene on zinc oxide: Characterization of surface-bound and gas-phase products and intermediates with FT-IR spectroscopy. *Journal of Molecular Catalysis A: Chemical*, *131*, 149–156.

Fehring, T. K., Christie, M. J., Lavernia, C., Mason, J. B., McAuley, J. P., MacDonald, S. J., & Springer, B. D. (2008). Revision total knee arthroplasty: Planning, management, and controversies. *Instructional Course Lectures*, *57*, 341–363.

Fehring, T. K., Odum, S., Calton, T. F., & Mason, J. B. (2000). Articulating versus static spacers in revision total knee arthroplasty for sepsis. *Clinical Orthopaedics and Related Research*, *380*, 9–16.

Fosco, M., Ayad, R. B., Amendola, L., & Tigani, D. D. (2012). Management of Bone Loss in primary and revision knee replacement surgery. *Recent Advances in Arthroplasty*, *1*, 387–95. https://doi.org/10.5772/26995

Frazer, R. Q., Byron, R. T., Osborne, P. B., & West, K. P. (2005). PMMA: An essential material in medicine and dentistry. *Journal of Long-Term Effects of Medical Implants*, *15*, 629–639. https://doi.org/10.1615/JLongTermEffMedImplants.v15.i6.60

Haas, S. S., Brauer, G. M., & Dickson, G. (1975). A characterization of polymethylmethacrylate bone cement. *The Journal of Bone and Joint Surgery. American Volume*, *57*, 380–391.

Horowitz, S. M., Gautsch, T. L., Frondoza, C. G., & Riley, L. (1991). Macrophage exposure to polymethyl methacrylate leads to mediator release and injury. *Journal of Orthopaedic Research*, *9*, 406–413.

Huan, Z., & Chang, J. (2007). Self-setting properties and in vitro bioactivity of calcium sulfate hemihydrate–tricalcium silicate composite bone cements. *Acta Biomaterialia*, *3*, 952–960.

Hvid, I., Christensen, P., Søondergaard, J., Christensen, P. B., & Larsen, C. G. (1983). Compressive strength of tibial cancellous bone. Instron and osteopenetrometer measurements in an autopsy material. *Acta Orthopaedica Scandinavica*, *54*, 819–825.

Ishikawa, K., Matsuya, S., Miyamoto, Y., & Kawate, K. (2007). *9.05 - Bioceramics. In Comprehensive Structural Integrity* (Vol. 9, pp. 169–214). Elsevier Ltd. https://doi.org/10.1016/B0-08-043749-4/09146-1

ISO 9917-1:2007. (2007). Dentistry—Water-based cements—Part 1: Powder/liquid acidbase cements.

Jiang, Y., Jia, T., Gong, W., Wooley, P. H., & Yang, S.-Y. (2013). Effects of Ti, PMMA, UHMWPE, and co-Cr wear particles on differentiation and functions of bone marrow stromal cells. *Journal of Biomedical Materials Research. Part A*, *101*, 2817–2825.

Kameda, T., Mano, H., Yamada, Y., Takai, H., Amizuka, N., Kobori, M., … Kumegawa, M. (1998). Calcium-sensing receptor in mature osteoclasts, which are bone resorbing cells. *Biochemical and Biophysical Research Communications*, *245*, 419–422.

Khader, B., Peel, S., & Towler, M. (2017 Sep). An injectable glass polyalkenoate cement engineered for fracture fixation and stabilization. *Journal of Functional Biomaterials*, *8*(3), 25.

Khoroushi, M., & Keshani, F. (2013). A review of glass-ionomers: From conventional glass-ionomer to bioactive glass-ionomer. *Dental Research Journal (Isfahan)*, *10*, 411–420.

Kim, M., An, S., Huh, C., & Kim, C. (2019). Development of zirconium-based alloys with low elastic modulus for dental implant materials. *Applied Sciences*, *9*, 5281.

Kim, M.-J., Kim, Y. K., Kim, K.-H., & Kwon, T.-Y. (2011). Shear bond strengths of various luting cements to zirconia ceramic: Surface chemical aspects. *Journal of Dentistry*, *39*, 795–803.

Kumar, C. Y., Nalini, K. B., Menon, J., Patro, D. K., & Banerji, B. H. (2013). Calcium sulfate as bone graft substitute in the treatment of osseous bone defects, a prospective study. *Journal of Clinical and Diagnostic Research*, *7*, 2926–2928.

Kuo, S.-T., Wu, H.-W., Tuan, W.-H., Tsai, Y.-Y., Wang, S.-F., & Sakka, Y. (2012). Porous calcium sulfate ceramics with tunable degradation rate. *Journal of Materials Science: Materials in Medicine*, *23*, 2437–2443.

Lazáry, Á., Balla, B., Kósa, J. P., Bácsi, K., Nagy, Z., Takács, I., … Lakatos, P. (2007). Effect of gypsum on proliferation and differentiation of MC3T3-E1 mouse osteoblastic cells. *Biomaterials*, *28*, 393–399.

Matsuya, S., Maeda, T., & Ohta, M. (1996). IR and NMR analyses of hardening and maturation of glass-ionomer cement. *Journal of Dental Research*, *75*, 1920–1927.

Murphy, S., Boyd, D., Moane, S., & Bennett, M. (2009). The effect of composition on ion release from ca-Sr-Na-Zn-Si glass bone grafts. *Journal of Materials Science. Materials in Medicine*, *20*, 2207–2214.

Nanda, S., Sood, N., Reddy, B. V. K., & Markandeywar, T. S. (2013). Preparation and characterization of poly(vinyl alcohol)-chondroitin sulphate hydrogel as scaffolds for articular cartilage regeneration. *Indian Journal of Materials Science*, *2013*, 1–8.

Newbury, D. E., & Ritchie, N. W. M. (2015). Performing elemental microanalysis with high accuracy and high precision by scanning electron microscopy/silicon drift detector energy-dispersive X-ray spectrometry (SEM/SDD-EDS). *Journal of Materials Science*, *50*, 493–518.

Nicholson, J. W. (1998). Chemistry of glass-ionomer cements: A review. *Biomaterials*, *19*, 485–494.

Nicholson, J. W. (2018). Maturation processes in glass-ionomer dental cements. *Acta Biomaterialia Odontologica Scandinavica*, *4*, 63–71.

Orellana, B. R., Hilt, J. Z., & Puleo, D. A. (2015). Drug release from calcium sulfate-based composites. *Journal of Biomedical Materials Research. Part B, Applied Biomaterials*, *103*(1), 135–142. https://doi.org/10.1002/jbm.b.33181

Peltier, L. F., Bickel, E. Y., Lillo, R., & Thein, M. S. (1957). The use of plaster of paris to fill defects in bone. *Annals of Surgery*, *146*, 61–69.

Qiu, Y. Y., Yan, C. H., Chiu, K. Y., & Ng, F. Y. (2012). Review article: Treatments for bone loss in revision total knee arthroplasty. *Journal of Orthopaedic Surgery (Hong Kong)*, *20*, 78–86.

Rabiee, S. M., Nazparvar, N., Azizian, M., Vashaee, D., & Tayebi, L. (2015). Effect of ion substitution on properties of bioactive glasses: A review. *Ceramics International*, *41*, 7241–7251.

Ross, A. C., Manson, J. E., Abrams, S. A., Aloia, J. F., Brannon, P. M., Clinton, S. K., … Shapses, S. A. (2011). The 2011 report on dietary reference intakes for calcium and vitamin D from the Institute of Medicine: What clinicians need to know. *The Journal of Clinical Endocrinology and Metabolism*, *96*, 53–58.

Sidqui, M., Collin, P., Vitte, C., & Forest, N. (1995). Osteoblast adherence and resorption activity of isolated osteoclasts on calcium sulphate hemihydrate. *Biomaterials*, *16*, 1327–1332.

Skripitz, R., & Aspenberg, P. (1999). Attachment of PMMA cement to bone: Force measurements in rats. *Biomaterials*, *20*, 351–356.

Stevens, C. M., Tetsworth, K. D., Calhoun, J. H., & Mader, J. T. (2005). An articulated antibiotic spacer used for infected total knee arthroplasty: A comparative in vitro elution study of Simplex® and Palacos® bone cements. *Journal of Orthopaedic Research*, *23*, 27–33.

Taïr, K., Kharoubi, O., Taïr, O. A., Hellal, N., Benyettou, I., & Aoues, A. (2016). Aluminium-induced acute neurotoxicity in rats: Treatment with aqueous extract of Arthrophytum (Hammada scoparia). *Journal of Acute Disease*, *5*, 470–482.

Thomas, M. V., & Puleo, D. A. (2009). Calcium sulfate: Properties and clinical applications. *Journal of Biomedical Materials Research Part B: Applied Biomaterials*, *88*, 597–610.

Thomas, M. V., Puleo, D. A., & Al-Sabbagh, M. (2005). Calcium sulfate: A review. *Journal of Long-Term Effects of Medical Implants*, *15*, 599–607. https://doi.org/10.1615/JLongTermEffMedImplants.v15.i6.30

Towler, M. R., Kenny, S., Boyd, D., Pembroke, T., Buggy, M., Guida, A., & Hill, R. G. (2006). Calcium and zinc ion release from polyalkenoate cements formed from zinc oxide/apatite mixtures. *Journal of Materials Science. Materials in Medicine*, *17*, 835–839.

Vaishya, R., Chauhan, M., & Vaish, A. (2013). Bone cement. *Journal of Clinical Orthopaedics and Trauma*, *4*, 157–163.

Walls, A. W. G. (1986). Glass polyalkenoate (glass-ionomer) cements: A review. *Journal of Dentistry*, *14*, 231–246.

Walls, A. W. G., McCabe, J. F., & Murray, J. J. (1988). Factors influencing the setting reaction of glass polyalkenoate (ionomer) cements. *Journal of Dentistry*, *16*, 32–35.

Wasson, E. A., & Nicholson, J. W. (1991). Studies on the setting chemistry of glass-ionomer cements. *Clinical Materials*, *7*, 289–293.

Williams, J. A., Billington, R. W., & Pearson, G. J. (2002). The effect of the disc support system on biaxial tensile strength of a glass ionomer cement. *Dental Materials*, *18*, 376–379.

Winkler, T., Sass, F. A., Duda, G. N., & Schmidt-Bleek, K. (2018). A review of biomaterials in bone defect healing, remaining shortcomings and future opportunities for bone tissue engineering. *Bone & Joint Research*, *7*, 232–243.

Woolford, M. J. (1989). The surface pH of glass ionomer cavity lining agents. *Journal of Dentistry*, *17*, 295–300.

Zheng, K., Lu, M., Rutkowski, B., Dai, X.-Y., Yang, Y., Taccardi, N., … Boccaccini, A. (2016). ZnO quantum dots modified bioactive glass nanoparticles with pH-sensitive release of Zn ions, fluorescence, antibacterial and osteogenic properties. *Journal of Materials Chemistry B*, *4*, 7936–7949.

How to cite this article: Hasandoost L, Alhalawani A, Rodriguez O, et al. Calcium sulfate-containing glass polyalkenoate cement for revision total knee arthroplasty fixation. *J Biomed Mater Res*. 2020;108B:3356–3369. https://doi.org/10.1002/jbm.b.34671